Use of Raman techniques in the analysis of archaeological sediments

Undergraduate thesis

Carmen Cano Fortún

Supervisor: Inocencio R. Martín Benenzuela

Co-supervisor: Carolina Mallol

Bachelor in Physics

Facultad de Ciencias

Universidad de La Laguna

17 May 2023

Acknowledgements

Firstly, I would like to express my gratitude to Kevin Soler, for his valuable and indispensable help in the laboratory and in understanding the fundamental concepts underlying this work. To Ada Dinckal, for his supportive attitude and assistance in comprehending archaeological concepts, and for his enthusiastic approach. I would also like to express my special appreciation to Inocencio R. Martín Benenzuela, for dedicating his time to this project, guiding me and resolving all my doubts. And thanks to Carolina Mallol for providing the original opportunity to work on this project and for extended contextual information on the archaeological contex.

Furthermore, I would like to express my gratitude to my parents and brother for their support when choosing my studies and their location, and, in general, to my entire family, including grandparents, aunts, uncles, godparents, and cousins, for their constant encouragement throughout my degree and the development of this undergraduate thesis. I am deeply grateful to my friends for their support during the long hours of study and in times of stress. In particular, I would like to express my appreciation to Lucía, Ainhoa, Paula, Paola, and Jova. Lastly, I would like to thank Ze'ev for his help and support despite the distance, and Ale for his ability to help me clear my mind.

Abstract

Raman spectroscopy has emerged as a well-established, non-destructive and versatile technique for studying archaeological cultural heritage. Lambrecht *et al.* (2021) introduced an analytical method utilizing Raman spectrum parameters of the D and G bands, as well as the valley between them, to discern whether char present in archaeological sites is derived from animals or plants. This approach is of great significance as it provides crucial insights into the lifestyles of prehistoric humans. In this study, a generalization of Lambrecht *et al.*'s methodology is proposed to offer a more efficient approach. Specifically, the ratios between Raman parameters (A_D, A_V and A_G) are represented in mappings for each area of interest within the samples. The values obtained are then compared to those of Lambrecht *et al.* (2021) for the distinction of the char origin. The results show that the proposed method effectively identifies char in large samples, albeit occasional ambiguity when classifying its nature. The latter could be addressed by adopting different measures such as taking a larger number of spectra at each point. Nevertheless, the method here proposed effectively identifies char in large samples, facilitating their interpretation, and thus offering a more convenient approach to such investigations. Overall, this study contributes to the advancement of archaeological research and the understanding of the cultural heritage through the application of Raman spectroscopy.

Keywords: Raman spectroscopy · Char · Charcoal · Animal chars · Archaeology

Resumen

La espectroscopía Raman ha ganado importancia en las útimas décadas en el ámbito de la arqueología, gracias a su naturaleza no destructiva y a su gran versatilidad. Lambrecht *et al.* (2021) introdujeron un método analítco basado en el cálculo de ciertos parámetros del espectro Raman, concretamente, de las bandas D y G y del valle entre ellas, que permite diferenciar si la materia carbonizada de yacimientos arqueológicos tiene naturaleza animal o vegetal. Esta propuesta es de gran importancia, ya que proporciona información sobre las formas de vida de los humanos en la prehistoria. En el presente estudio, se propone una generalización del método desarrollado por Lambrecht *et al.* (2021) para intentar desarrollar un enfoque más eficiente. Concretamente, se representan mapas de ratios calculados entre los parámetros Raman (A_D, A_V y A_G) para cada área de interés de las muestras bajo estudio. Después, los valores obtenidos se comparan con los de Lambrecht *et al.* (2021) para la diferenciación del origen de la materia carbonizada. Los resultados muestran la eficacia del método propuesto a la hora de identificar dicha materia en las muestras, con ocasional ambigüedad en los resultados a la hora de diferenciar la naturaleza de dicha materia. Esta ambigüedad puede minimizarse adoptando medidas como, por ejemplo, tomar más espectros en cada punto. Sin embargo, el método propuesto es capaz de resolver la presencia de materia carbonizada, facilitando la interpretación de las muestras y, por tanto, ofreciendo un enfoque más cómodo para las investigaciones en este ámbito. En conclusión, este estudio contribuye al avance en la investigación arqueológica y en la comprensión del patrimonio cultural a través de la espectroscopía Raman.

Palabras clave: Espectroscopía Raman · Materia carbonizada · Carbón · Materia carbonizada animal · Arqueología

Contents

1 Introduction

Resumen

En esta sección inicial, se presenta una primera aproximación a los conceptos fundamentales relacionados con el efecto Raman y la espectroscopía Raman. Se proporciona una explicación detallada del funcionamiento del microscopio confocal Raman, que se utilizará en el presente trabajo para llevar a cabo el análisis de las muestras. Posteriormente, se introduce el uso de la espectroscopía Raman en el campo de la arqueología, se exploran sus inicios y su evolución a lo largo del tiempo, y se concluye con su aplicación específica en la investigación de muestras arqueológicas que han experimentado procesos de combustión. Por último, se describe brevemente la estructura del estudio llevado a cabo en el presente trabajo.

This section is intended to provide a brief introduction to the concept of Raman spectroscopy and to its applicability in the field of archaeology, as well as to undertake an approach to the contents of this study.

1.1 Raman effect and Raman spectroscopy

When a sample is illuminated by a monochromatic light beam, most of it is either absorbed, reflected or transmitted by the sample. However, a small fraction of the photons interact with the sample. These photons can be scattered either elastically or inelastically. Predominantly, light is elastically scattered, i.e., there is no change in the photon energy, which is known as Rayleigh scattering. Conversely, inelastic scattering occurs when the energy of the scattered photon is not equal to that of the incident photon. This is known as Raman effect [1]. Specifically, if the interaction causes the photon to gain vibrational energy, the scattered light will have higher frecuency than that of the incident beam, which is referred to as anti-Stokes Raman scattering. When the photon loses energy and the scattered light has a lower frecuency than the incident light, the process is known as Stokes Raman scattering [2]. These three types of phenomena are depicted schematically in Figure 1.

The wavelength shift of scattered radiation depends upon the chemical structure of the molecules responsible for it, each one possessing a unique spectral fingerprint. Raman spectroscopy employs the scattered light to gather information regarding molecular vibrations, thereby providing insights about their structure and symmetry and enabling both quantitive and qualitative analysis of the individual compounds, and thus the

chemical composition of the sample [2] [3] [4]. This spectroscopic technique offers several advantages, including its versatility for use not only with gases but also with liquids and solids, as well as its non-destructive nature and the lack of a requirement for sample preparation.

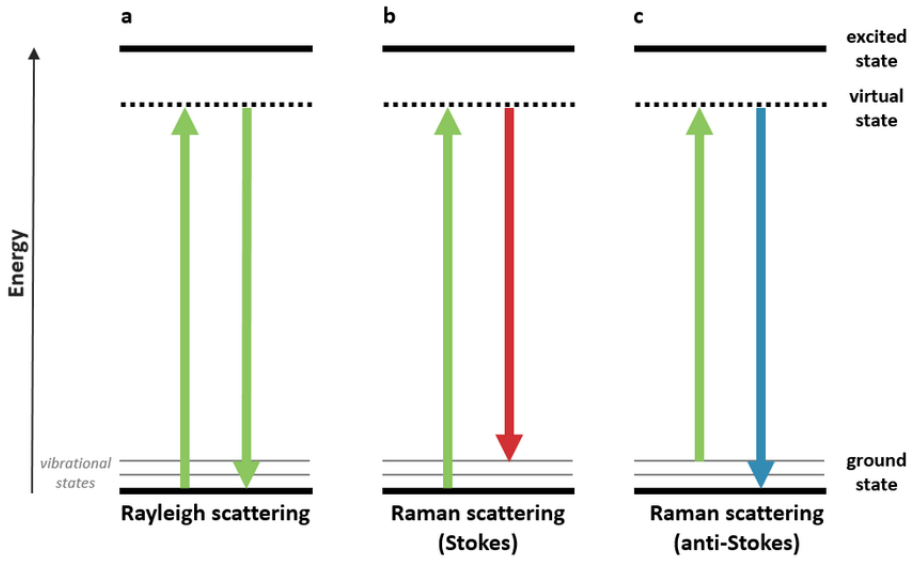

Figure 1: Schematic illustration of the processes involved in Rayleigh scattering, Stokes Raman scattering, and anti-Stokes Raman scattering when matter interacts with light.

On the other hand, confocal microscopy is commonly utilized along with Raman spectroscopy. The essential components of confocal microscopes are pinhole apertures. Figure 2a presents a schematic representation of the distinctions between a conventional microscope and a confocal one. The laser beam is focused on the sample through the microscope objective, the light emitted by the excited molecules is then collected by the objective lens and focused by a second lens through the pinholes. The apertures ensure that only the light emitted at the focal point is captured by the detector, while the emission from above or below the focal plane is blocked [5]. In confocal Raman microscopy, the filtered backscattered Raman signal is detected by a spectrometer and dispersed on a CCD (charge coupled device) camera to produce the spectrum [2]. A schematic illustration of the optical layout is presented in Figure 2b. The combined application of these techniques is of notable significance since it enables visual examination of samples at high magnification, which in turn permits selective analysis of specific areas as small as 1 μm in diameter [6]. This capability has resulted in an increased application of microconfocal Raman spectroscopy in recent times.

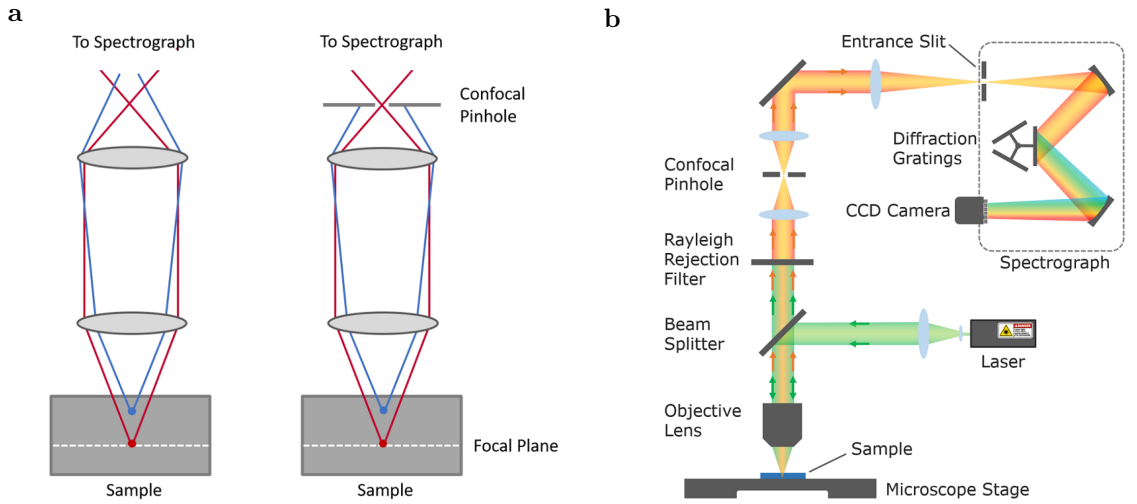

Figure 2: **a** Differences in operation between a classic microscope (left) and a confocal microscope (right). **b** Optical layout of a Confocal Raman Microscope.

1.2 Overview of Raman spectroscopy in archaeology

While the Raman effect was first discovered in 1928, it was not until the 1970s that the technique began to be employed for the analysis of works of art, such as paintings and vessels, with the introduction of the MOLE Raman microprobe (Molecular Optical Laser Examiner). Shortly after, reports on pigment composition determination on manuscripts emerged. Researches found that Raman spectroscopy was a non-destructive technique, and as it developed and became more widely available, archaeologists began to explore its use in identifiying ancient materials, such as textiles, as well as determining the composition of archaeological objects, including ceramics and metals [7] [8] [9].

Nowadays, analytical Raman spectroscopy has become a well-established technique for the characterization of cultural heritage artefacts, among other materials. It is commonly employed either in isolation or in conjunction with other techniques to provide crucial information for both investigative and preservation purposes. The data obtained from Raman spectroscopic analysis provides valuable insights into the constituent materials, their proportions, provenance, presence of unusual materials, indications of degradation or deterioration, and authenticity of the artefacts [10].

1.3 Raman spectroscopy in investigation of archaeological combustion contexts

In the study of prehistoric humans lifestyles, the characterisation of char can yield crucial information. 'Char' refers to solid residues resulting from the carbonization process, that is, is a product of heating biomass in a low-oxygen environment. Under such

conditions, the biomass undergoes a loss of hydrogen, oxygen and nitrogen, resulting in an increase in its carbon content and leading to the development of an aromatic molecular structure. Thus, the investigation of chars, such as charcoal or charred meat and fat found in anthropogenic fireplaces, can provide valuable data on the type of fuel used and the eating habits of the ancient occupants [11].

In keeping with the matter at hand, microRaman spectroscopy is notably sensitive to the aromatic nanostructure of carbon compunds. This, combined with its non-destructive nature, makes it particularly well suited to the study of archaeological chars.

Specifically, a Raman spectrum of char is mainly characterised by two bands called the G and D bands. The G band, located at about $1600 - 1700\, cm^{-1}$, corresponds to the vibrational modes of the hybridized carbons of the aromatic rings. It is the only vibration that is Raman active in ideal graphite crystals and therefore, the term 'G' stands for graphite. On the other hand, the D band is located at approximately $1350\, cm^{-1}$ and is associated with the vibrational modes of the edges of the aromatic rings and it is caused by a double resonance effect created by defects in the ideal graphite structure. The term 'D' stands for disorder. Hereby, upon initial observation, the existence of char in a sample can be readily identified by the presence of these two bands in its spectrum [11] [12].

Additionally, the Raman spectrum can provide information regarding the nature of the organic precursor. When analyzing spectra corresponding to char, the intensities, positions, and bandwidths are dependent on its nanostructure which, in turn, is influenced by the charring temperature and the chemical composition of the organic precursor [13]. Thereby, through a comprehensive analysis of the Raman spectrum, it is possible to differentiate between the animal and vegetal origin of the organic precursor.

With the aim of achieving this differentiation, Lambrecht *et al.* (2021) [12] plotted some of the Raman spectra parameters and investigated their distinct trends in both types of matter. Specifically, they determined the values of the intensity at the spectrum peaks, denoting H_G the intensity peak corresponding to the Graphite band and H_D that of the Disorder band, as well as the value of the valley between them, H_V (Figure 3). The ratios H_V/H_G and H_D/H_G were then computed, and the positions of the G and D bands were plotted against both ratios. This analysis yielded particularly effective results for the G band and the H_V/H_G ratio in differentiating between the animal and vegetal origin. The main findings which they obtained for the G band and both ratios can be seen in Figure 4a-b.

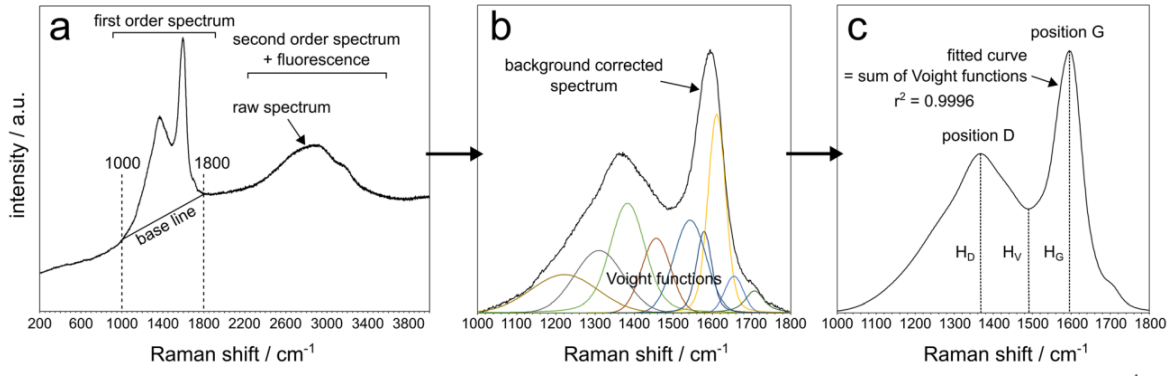

Figure 3: Method for Raman spectra processing and extraction of parameters followed by Lambrecht *et al.* (2021) [12]: subtraction of a baseline, background-corrected spectrum fitted with an arbitrary number of Voight functions and measurement of Raman parameters on fitted curve.

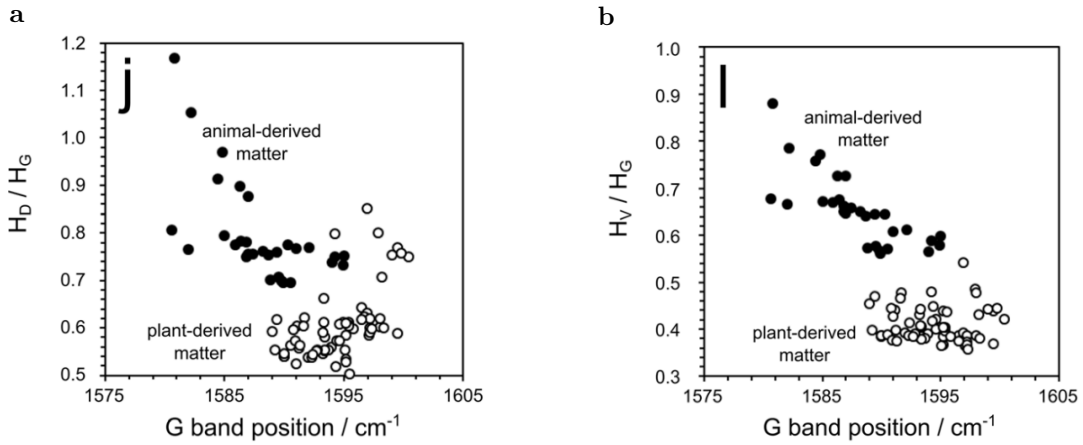

Figure 4: Results obtained by Lambrecht *et al.* (2021) [12] for the furnace and outdoors experiments: **a** Results for the H_D/H_G ratio against the position of the G band. **b** Results for the H_V/H_G ratio against the position of the G band.

Hence, in Figure 4a-b, it can be noticed that for the H_D/H_G ratio, plant-derived matter values were within the range of $0.5 - 0.85$, being predominantly between $0.5 - 0.65$, whereas animal-derived matter exhibited values ranging from 0.65 to 1.2, with the highest concentration being between 0.65 and 0.8. Similarly, the H_V/H_G ratio shows that plant-derived matter had values ranging between 0.3 and 0.6, while animal-derived matter presented values within the range of 0.5 and 0.9. These results can be seen summarized in table 1.

Table 1: Results obtained by Lambrecht *et al.* (2021) [12] for the values of the A_D/A_G and A_V/A_G ratios when differentiating the nature of charred organic material.

Matter	H_D/H_G	H_V/H_G
Animal-derived	$0.65 - 1.2$	$0.5 - 0.9$
Plant-derived	$0.5 - 0.85$	$0.3 - 0.6$

1.4 Present study

The present investigation aims to apply the methodology described by Lambrecht *et al.* (2021) [12] to large areas. To achieve this, microconfocal Raman spectroscopy will be employed to analyze the samples. The resulting spectra will then be examined to generate intensity and ratio maps, followed by the differentiation of the origin of any organic matter present within the samples. This distinction will be performed using the ranges outlined in Table 1. Finally, a discussion regarding the obtained results will be made. This section will explore the potential factors that could have influenced the outcome, such as the sample's orientation concerning the laser beam, the degradation of the char present in the samples through the process of oxidation over extended periods of time and methodological influences.

2 Objectives

Resumen

En este apartado se introducen los principales objetivos del estudio, destacando el propósito de desarrollar un nuevo método experimental que permita el análisis y clasificación de materia orgánica carbonizada en muestras de cualquier tamaño.

The primary aims of this study are:

1. To develop an experimental method, based on Raman techniques, that allows for differentiation of the presence of charred organic materials in large study areas of archaeological sediments.

2. To analyze two different samples, focusing on specific areas of interest, and identify the presence of char on them, if any.

3. To determine the animal or plant-derived origin of any charred organic material detected.

3 Materials and methods

Resumen

A lo largo de esta sección se hace una breve descripción del método seguido para la extracción de las muestras en el yacimiento arqueológico, así como las medidas adoptadas para su transporte y su posterior preparación en el laboratorio para facilitar el trabajo con ellas. A continuación, se ofrece una breve introducción a las muestras que serán objeto de estudio a lo largo del trabajo. Por último, se proporciona una explicación detallada de la metodología empleada en el análisis de las muestras, haciendo hincapié en el proceso de adquisición de los espectros Raman y en el posterior análisis de los datos.

In this section, a description of the samples and their preparation, as well as the experimental methodology employed for their analysis, will be provided.

3.1 Preparation of the samples

The samples were collected in The Birnik National Historic Landmark located in Alaska. The blocks were stabilized for transport using plaster-of-Paris bandages or toilet paper and packaging tape. Figure 5 provides an illustration of this process, although it depicts samples unrelated to those employed in the present study, it serves to provide a general understanding of the methodology utilized.

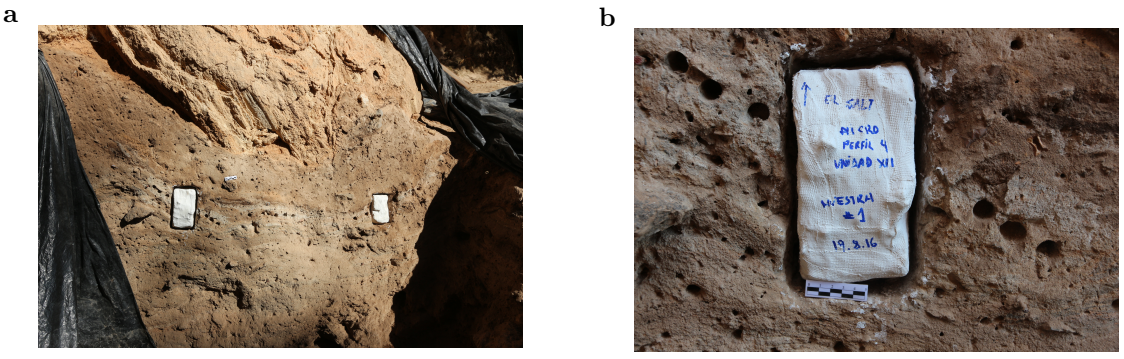

Figure 5: Pictures of the collection process of samples in the archaelogical site of El Salt: **a** Profile with the samples. **b** Sample packaging for transportation.

In the laboratory, the samples preparation was made following the standard method used in the AMBI Lab, described by Leierer *et al.* (2019) [14]. The intact sediment blocks were dried in an oven at 60 ^{o}C for at least 48 hours. Next, they were impregnated with a mixture of polyester resin (Palatal strained resin UN1866, TNK composites), styrene

(Styrene monomer (CAS: $100-42-5$) UN2055, TNK composites) and a catalyser (Methyl−ethyl−ketone (Luperox, CAS: $78-93-3$), TNK composites) in a ratio of 7:3:0,1. After hardening, the blocks were cut into $1\,cm-$thick slabs using a Euro-Shatal M31100 radial saw, glued onto $9\,cm$ x $6\,cm$ glass slides and then trimmed to $1\,mm$ thickness by using a Uniprec ATA Brilliant−220 precision cutting machine. Finally, the samples were grinded to $30\,\mu m$ thickness with a G&N MPS-RC-Geology grinding machine.

The final step is to position the samples onto the support in order to take the measurements. This support consists of a single 3D-printed piece with two thin protrusions on either side, on which the sample rests, and three screws that enable adjustment of the sample and which mantain its stability. Moreover, to prevent damage to the sample, small pieces of foam are placed in areas of contact with the screws. The support and final setup can be seen in Figure 6a-b.

a **b**

Figure 6: **a** Sample support for the measurements. **b** Colocation of the sample in the support, using three small foam pieces in order to avoid damage to the sample.

3.2 Samples

This work is focused on the analysis of two samples. The first one corresponds to Alaska Sm13 Bottom and will be referred to as *Sample 1* from now over. This sample presents three main zones which might have charred organic material and, hence, are of archaelogical interest. In these areas is where the study was focused and they can be seen in Figure 7 framed in different colours.

The second sample, which will be referred to as *Sample 2*, corresponds to Alaska Sm13 Top. In this case, the study was focused on four main areas, shown in Figure 8.

In the next section, a detailed explanation of the method followed to analyse both samples will be made.

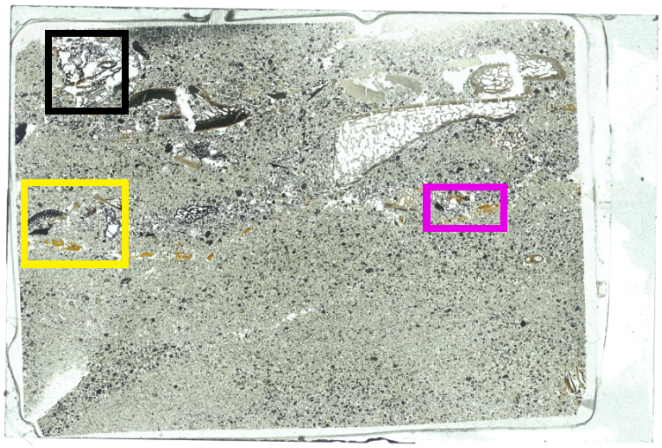

Figure 7: Sample 1 (Alaska Sm13 Bottom) with the zones of interest framed in colours.

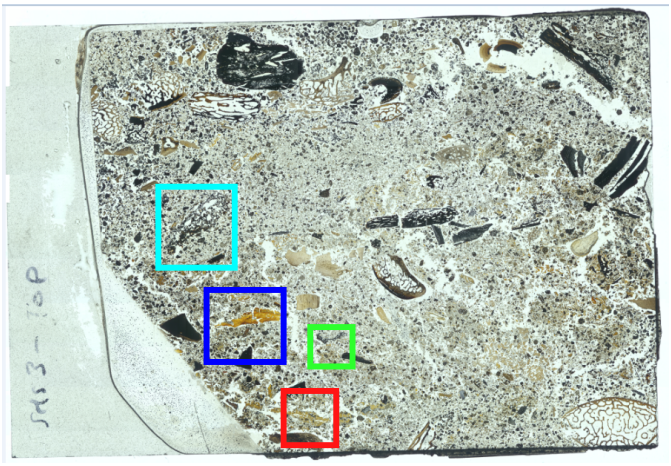

Figure 8: Sample 2 (Alaska Sm13 Top) with the zones of interest framed in different colours.

3.3 Acquisition and processing of Raman spectra

Raman spectra were acquired with a Renishaw InVia^{TM} confocal Raman microscope, located at the Department of Physics and IMN of the University of La Laguna (ULL), Tenerife, Spain. The samples were excited with a $532\,nm$ (green) laser focused on the sample surface. The Raman signal was collected in backscattered mode using a $20x$ objective. The analyzed sampled volume in each measurement was a few cubic micrometres, and the laser power on sample was kept low to avoid its degradation. The diffraction grating was $1800\,/mm$, which produced spectral resolution of $1.73\,cm^{-1}$. The Raman shifts were acquired from 700 to $2400\,cm^{-1}$. In Lambrecht *et al.* (2021) [12],

two sets of 57 and 108 spectra were recorded in every point of interest with $3\,x\,10\,s$ of acquisition time. However, given the high number of spectra required to measure a large map of the sample, sets of only 2 spectra were recorded in each point with $1\,s$ acquisition time, to cut back on the overall measuring time.

In Figure 9a-c are shown the typical spectra obtained in presence of char, as well as the procedure to extract the Raman parameters. Spectra were processed using Python. After acquiring a raw spectrum, the data was smoothed by applying the Savitzky-Golay filter (Figure 9a), whose number of convolution parameters were chosen based on the best fit to the signal-to-noise ratio of the spectra. These parameters determine the window length of the filter, i.e., the number of data points used to fit the polynomial at each point in the signal. Then, a straight baseline was selected between 1100 and 1800 cm^{-1} (Figure 9b) and subtracted to the smooth data. Once we had the baseline-corrected data, the positions of the D ($\sim 1360\,cm^{-1}$) and G ($\sim 1600\,cm^{-1}$) bands, which correspond to the two peaks of the curve respectively, as well as that of the valley ($\sim 1500\,cm^{-1}$) were calculated. After this, three sections of 40 points, centred on the three recorded positions, were selected and the areas of these sections were integrated (Figure 9c). The parameters obtained were labelled as follows: A_D for the Disorder area, corresponding to the first peak; A_V for the area of the valley and A_G for the Graphite area, corresponding to the second peak. From these areas, three ratios were calculated: A_V/A_D, A_D/A_G and A_V/A_G. This approach of calculating the ratios with the areas values rather than using single point values was employed in order to minimize the impact of the noise in the signals.

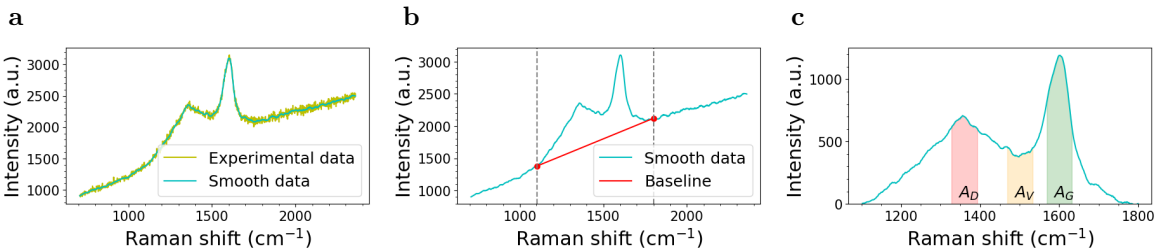

Figure 9: Raman spectral processing and extraction of parameters: **a** Smoothing of the raw Raman spectrum with the Savitzky–Golay filter. **b** A baseline for the smooth data is chosen between 1100 and 1800 cm^{-1}. **c** Spectrum after background fluorescece removal and measurement of the Raman parameters.

Subsequently, with the purpose of differentiating the areas of the sample where there is presence of charred organic material, as well as its nature, four mappings were made: a map of the intensities and maps of the A_V/A_D, A_D/A_G and A_V/A_G ratios.

First, a map of the intensities was obtained by choosing the intensity value associated with 2225 cm^{-1} on the Raman shift for each data point (Figure 11a). Figure 10a-c shows the other types of spectra which can be obtained apart from that of the presence of char. Here it can be seen that when saturation of the CCD occurs (Figure 10c), the values of the intensity are much higher than on the other cases. However, it also shows that they can be 0 from a certain value of the Raman shift. In Figure 9a, it can be noticed that the Raman spectrum in presence of char has the lowest intensity values among the four different cases, being its maximum value around 4000 $a.u.$ Due to the large number of points and the wide range of intensity values, distinguishing between points with the presence of char and those that are saturated with a value of 0 was difficult, as the gradient colour of the maps could not clearly differentiate between intensities under 10000 $a.u.$ In order to avoid misinterpretation, a selection of the points with intensity 0 and above 100000 $a.u.$ was made, giving them the value 100000 $a.u.$ This narrowed the range of intensity values, which allowed a greater differentiation between the colours of low intensity pixels. The remaining points with low intensity values are likely to be the ones with presence of char. The resulting map is shown in Figure 11b.

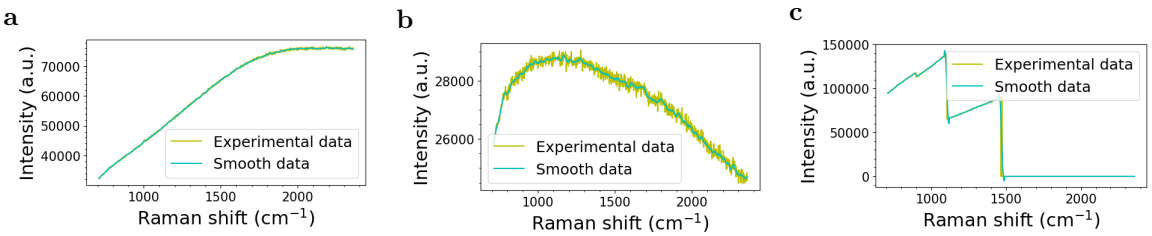

Figure 10: Other types of Raman spectra obtained: **a** Background fluorescence, Raman spectrum without presence of charred organic matter. **b** Artifact. **c** Raman spectrum when saturation of the CCD occurs.

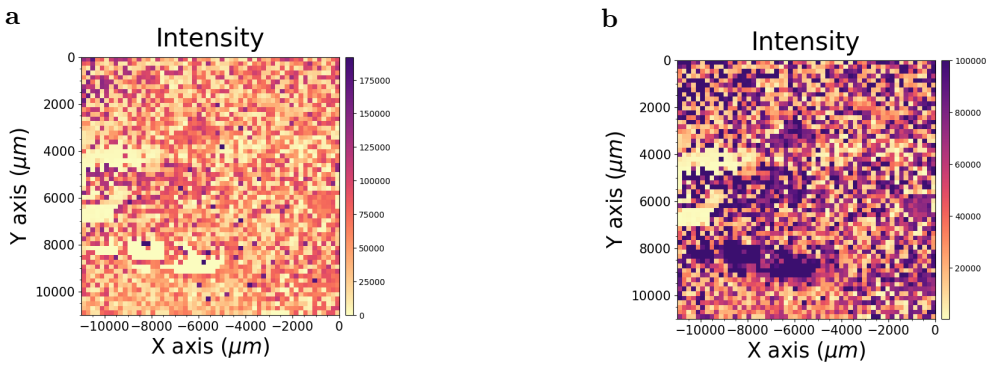

Figure 11: Maps of intensity for the yellow-framed area in Sample 1: **a** Map of integrated intensity. **b** Map of integrated intensity with a selection of saturated points made.

Then, to assure the presence of organic matter, the values of the three calculated ratios (A_V/A_D, A_D/A_G and A_V/A_G) were represented in three separated maps, as shown in Figure 12a. In order to better differentiate the points which might present char, a selection of the values above the threshold 1.5 for A_V/A_D and A_D/A_G ratios, and above 2 for A_V/A_G ratio, was made, giving them the value of the respective limit (Figure 12b).

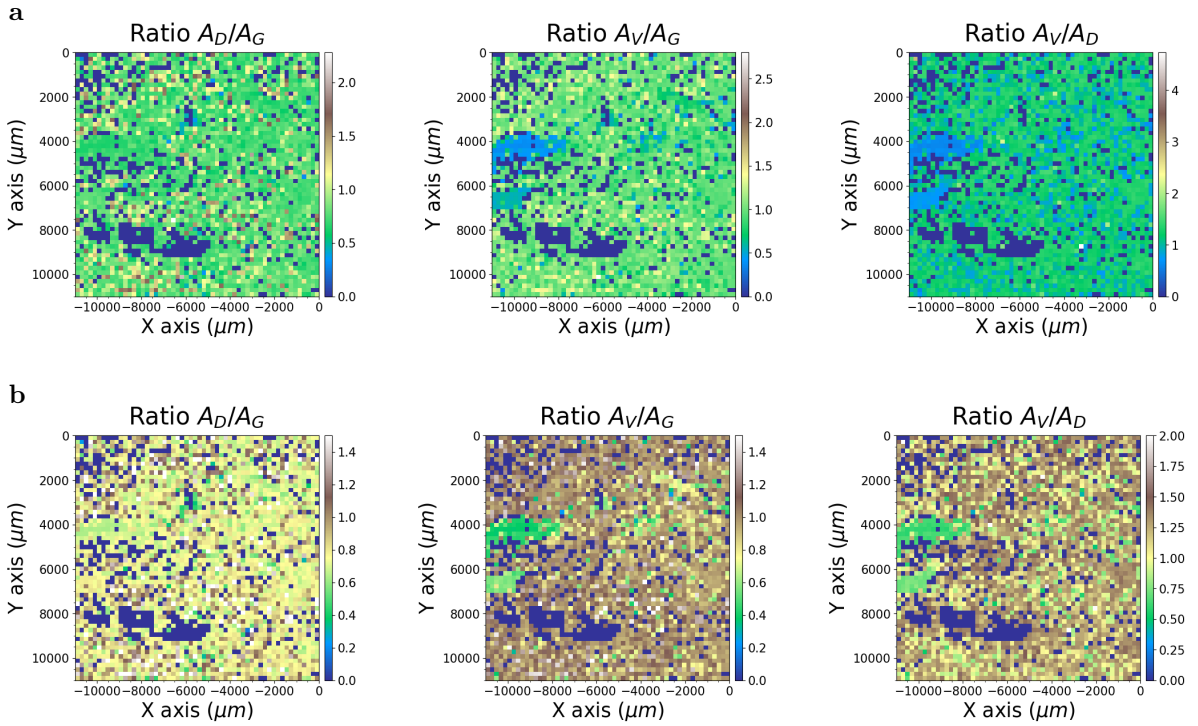

Figure 12: Ratio maps for the yellow-framed area in Sample 1: **a** Maps of the ratios calculated from the Raman parameters A_D, A_V and A_G. **b** Maps of the ratios where a selection of high values was made so that the different areas are better distinguished.

From Figure 9, it is noticeable that the ratio between the integrated intensity of the valley and the peaks is only lower than 1 in the presence of char. Particularly, to differentiate the areas likely to contain char, the A_V/A_D ratio is deemed to be the most reliable. It is possible that the Raman spectrum may present a peak due to the luminiscence of the resin, noise of the data or unkown source, which could lead to incorrect results of the A_V/A_G and A_D/A_G ratios, as they only consider an increasing trend in the spectrum. In contrast, the A_V/A_D ratio calculates the value between the valley and the Disorder area, and therefore, it measures a decreasing trend on the spectrum which could only occur at those Raman Shift values if char is present. This is the reason why, to differentiatie the areas likely to have char, the intensity map will first be analyzed to identify low values, followed by the A_V/A_D ratio map. If this two indicators suggest the presence of char, a more detailed study will be made using the A_D/A_G and A_V/A_G ratios. Nonetheless, as can be seen in Figure 12b and as subsequent

sections will illustrate, the ratio A_D/A_G often yields ambiguous results, and thus, the conclusive ratio will typically be the A_V/A_G.

Taking this into account, the laser power applied to the sample was adjusted using the multiple maps. Two power values were utilized during the measurements, and the resulting maps are shown in Figure 13a-d. The intensity map obtained at 5% power (Figure 13b) presents a higher number of saturated points compared to the intensity map obtained at 1% power (Figure 13a), which could lead to a loss of critical data concerning the presence of char. However, when attending to the ratio maps, it is noticeable that the saturated points in the 5% power maps (Figure 13d) correspond to high-value points

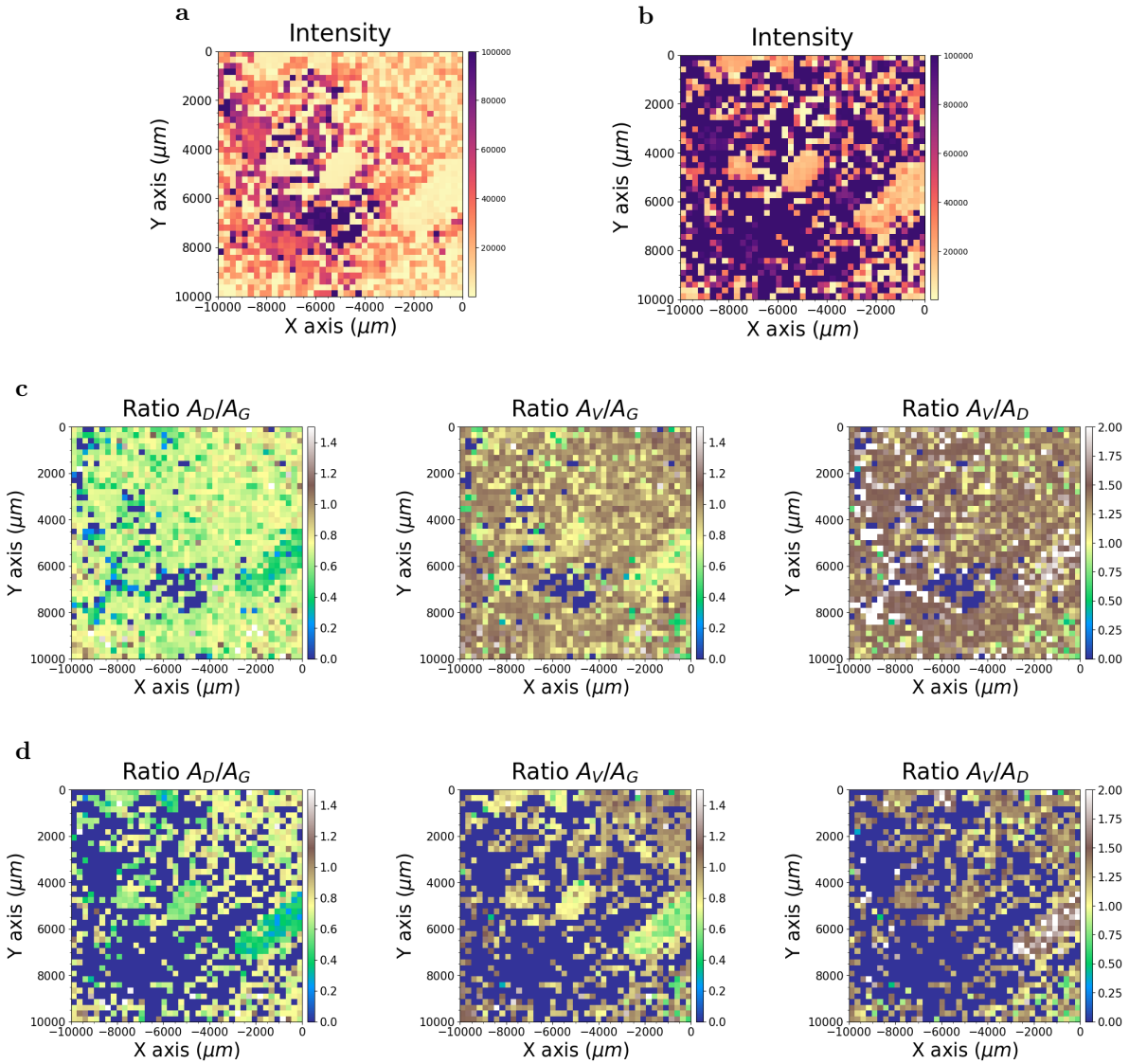

Figure 13: Maps of the black-framed area in Sample 1 for two laser power values: **a** Integrated intensity resulting of using the laser at 1% power. **b** Integrated instensity when the laser was used at 5% power. **c** A_D/A_G, A_V/A_G and A_V/A_D ratio maps for 1% power of the laser. **d** A_D/A_G, A_V/A_G and A_V/A_D ratio maps when 5% power of the laser was used.

on the ratios of 1% power maps. Thus, as only pixels with ratio values less than 1 are likely to have char, it can be inferred that the saturated points cannot correspond to zones with charred organic matter. This is further supported by the intensities maps where, as previously mentioned, char presents very low intensity values. As shown in Figure 13a-b, the saturated points at 5% power correspond to points with medium to high intensity in the 1% power map and, hence, they cannot correspond to data of char.

This trend was observed in several measurements, leading to the conclusion that applying a 5% power to the sample results in more saturated points but does not cause a loss of critical data. In fact, it could streamline the differentiation of areas which are likely to contain charred organic material, as the contrast between the values in the maps increases. Consequently, for the remaining measurements, the power on the sample was kept at 5%, avoiding its degradation and optimize the distinction of zones with charred organic material.

4 Results

Resumen

En esta sección se exponen los resultados obtenidos para las diversas zonas de las dos muestras. Para ello, se realiza una breve descripción de cada una, seguida de la presentación de los mapas de intensidad y ratios correspondientes. Asimismo, al comienzo de los resultados de cada muestra, se proporciona una tabla resumida que contiene los valores numéricos de los ratios para cada área de interés en la misma.

The following section is dedicated to present the results obtained for each area of interest in both samples. A brief description of these results will be provided, along with visual representations of the same.

4.1 Sample 1

In order to provide a clearer overview of the areas in Sample 1 where presence of charred organic material was found, the results are summarized in Table 2. Subsequently, a detailed account of the results obtained for each zone will be provided over the course of this section.

Table 2: Values of the A_D/A_G and A_V/A_G ratios for the zones in Sample 1 where charred organic material was found. In the first column, the term "High res. measure" refers to the results of a high-resolution measurement taken in a small zone of the corresponding area where the presence of charred organic material was likely, in order to confirm its existence. The last two columns correspond to the peak values of the distribution spectra made with the ratio values for each zone.

Section	A_D/A_G	A_V/A_G	A_D/A_G dist. peak	A_V/A_G dist. peak
Red framed zone (Yellow area)	$0.6 - 0.7$	$0.4 - 0.6$	0.67	0.46
Blue framed zone (Yellow area)	$0.65 - 0.85$	$0.5 - 0.7$	0.81	0.63
Orange framed zone (Yellow area)	$0.6 - 0.8$	$0.2 - 0.45$	0.63	0.3
Black area (High res. measure)	$0.6 - 0.8$	$0.25 - 0.8$	0.7	0.55

4.1.1 Yellow area

In the intensities map of this area, shown in Figure 11b, different zones can be distinguished, including areas with many saturated or close to saturated points (coloured dark purple) and areas with low intensity (close to beige) and, hence, likely to have organic matter. Within the latter group, two main areas presented promising intensity values and are shown framed in red and blue in Figure 14.

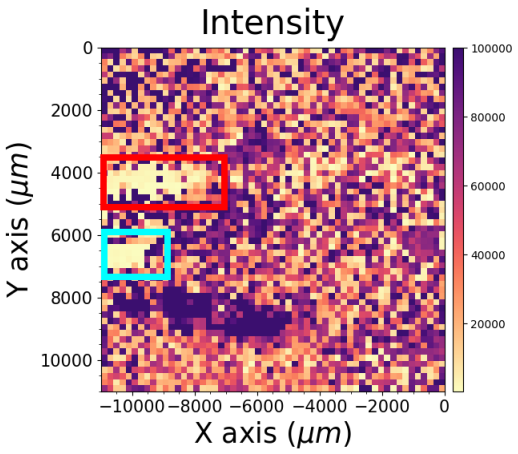

Figure 14: Map of integrated intensity for the yellow zone in Sample 1. The two framed areas are likely to have presence of charred organic material.

In section 3.3 it was analyzed that only points with values of the ratios below 1 could present char. Thus, the ratio maps (shown in Figure 12b) suggest that the same two areas discussed in the intensities map may contain charred organic matter, as indicated by their colour, which corresponds to values below 1. A clearer picture of the two zones is shown in Figure 15, where they can be seen framed in red and blue in the A_V/A_G ratio map and in a photograph of this sample.

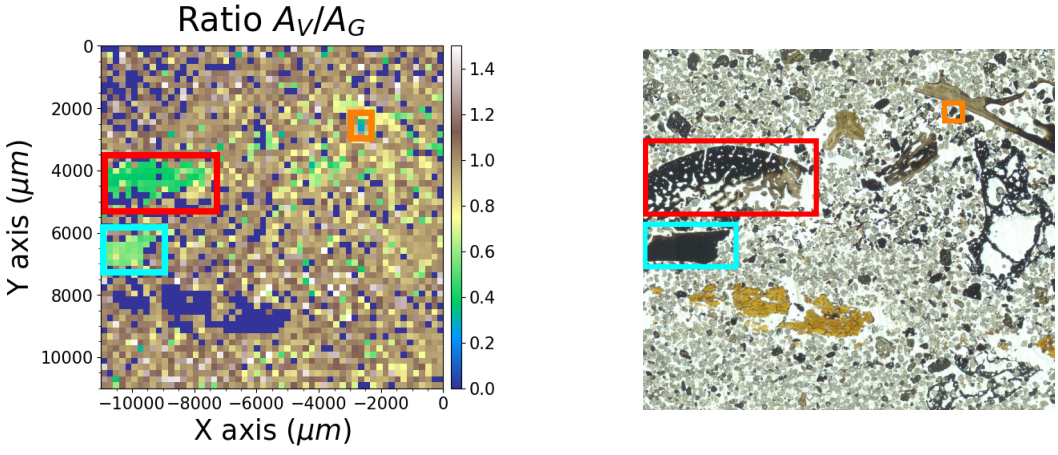

Figure 15: Zones with presence of char in the yellow-framed area of Sample 1.

More concretely, the area framed in red presented values between 0.4 and 0.6 for the ratio A_V/A_G and between 0.6 and 0.7 for the A_D/A_G. The blue-framed area had values between 0.5 and 0.7 for the A_V/A_G ratio, and between 0.65 and 0.85 for the A_D/A_G ratio. Based on these values, it can be safely affirmed that there is presence of charred organic material in these two areas.

In Figure 16a-b the distribution spectra of the ratio values for both zones are shown. The peaks of the distributions for the red-framed area were approximately 0.46 for the A_V/A_G ratio and approximately 0.67 for the A_D/A_G ratio. In regard to the area framed in blue, the distributions had their maximums at around 0.63 for the A_V/A_G ratio and around 0.81 for the A_D/A_G ratio. These results demonstrate a clear difference in the trend of the two areas, with the red-framed area having lower values for both ratios compared to the blue-framed area.

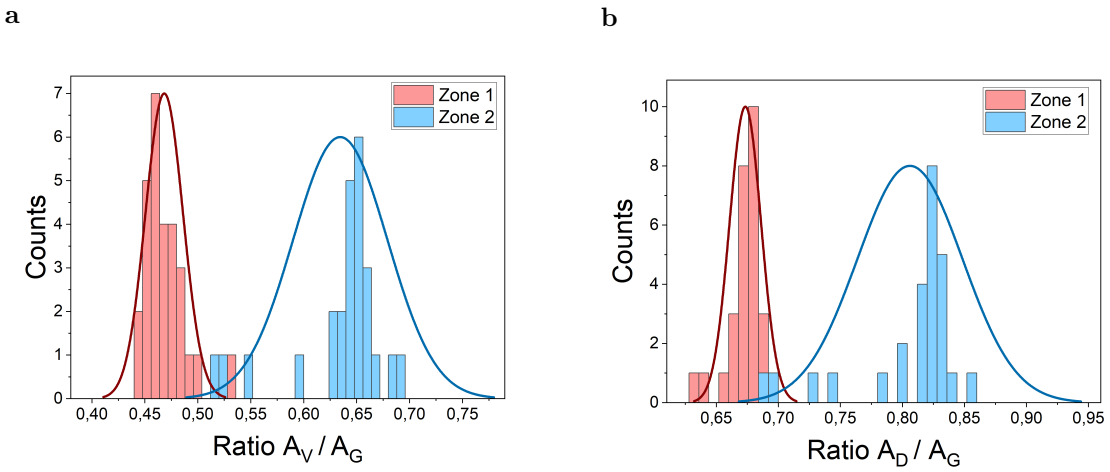

Figure 16: Distribution spectra for the ratio values of the red and blue-framed zones in the yellow area of Sample 1, where *Zone 1* refers to the area framed in red, while *Zone 2* refers to that framed in blue: **a** Ratio A_V/A_G. **b** Ratio A_D/A_G.

On the other hand, in Figure 15, it can also be appreciated several scattered points with potential presence of char, as suggested by their colours. With the purpose of confirming the presence of organic matter in these sorts of areas, a high resolution measurement was taken in a small region with particularly interesting values of the ratio, which can be seen framed in orange in Figure 15. After the analysis, it was observed that this area presented the characteristic spectrum of char, with values of the A_V/A_G ratio between 0.2 and 0.45 and of the A_D/A_G between 0.6 and 0.8. A distribution spectrum was made for each ratio of this area, following the same procedure as in the previous case, and the peak of the distribution for the A_V/A_G ratio was observed to be around 0.3, whereas that of the A_D/A_G ratio was at around 0.63 (Figure 17).

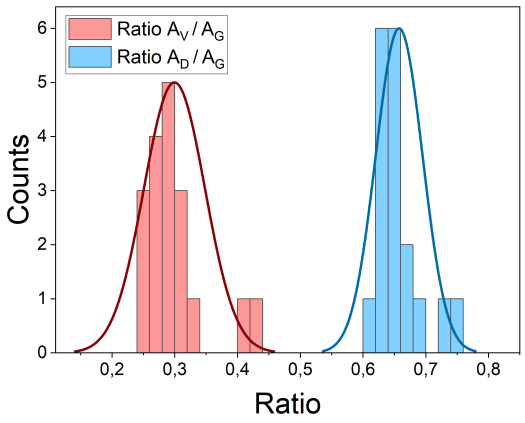

Figure 17: Distribution spectra for the ratio values of the orange-framed area in the yellow zone of Sample 1. The spectrum of each ratio (A_V/A_G and A_D/A_G) is represented in different colours.

To conclude, compared to the blue and red-framed areas, the area framed in orange exhibited lower values for both ratios, with the A_V/A_G ratio being notably lower. As a result, the distribution peaks for both ratios in this zone were at lower values than in the other two areas. However, the differences were less pronounced with the red-framed area than with the blue one.

4.1.2 Black area

The main results for this area are shown in Figure 13. A map of the integrated intensity, the A_V/A_D ratio and a closer picture of the zone are shown in Figure 18. Here it can be appreciated that only a small area, located on the bottom right and framed in light blue, has values of the intensity and the ratio which might correspond to charred organic matter. To asssure it, a higher-resolution measurement was taken in this small zone.

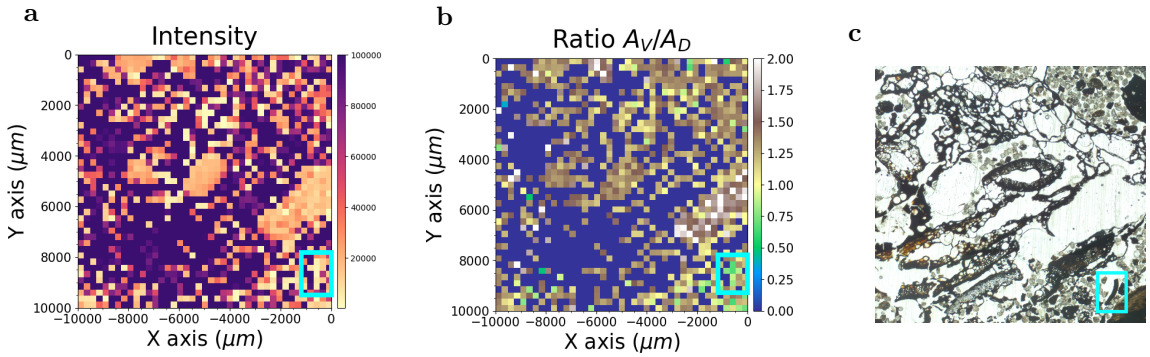

Figure 18: **a** Map of the integrated intensity for the black-framed area in Sample 1. The area framed in light blue is likely to have char. **b** Map of the A_V/A_D ratio for the same zone with the area likely to have char framed in light blue **c** Photograph of the black-framed zone in Sample 1 with the small area of interest framed.

The maps resulting of the high-resolution measurement are shown in Figure 19b and Figure 20a-c. These results indicate that, indeed, the area of study has presence of char, particularly the zone framed in colour. Plotting a distribution spectrum of the ratio values for the A_V/A_G map of this zone (Figure 21), we observe that it presents values between 0.25 and 0.8, having its peak around 0.55. With regard to the A_D/A_G distribution spectrum, it had values ranging from 0.6 to 0.8, being the distribution peak at 0.7.

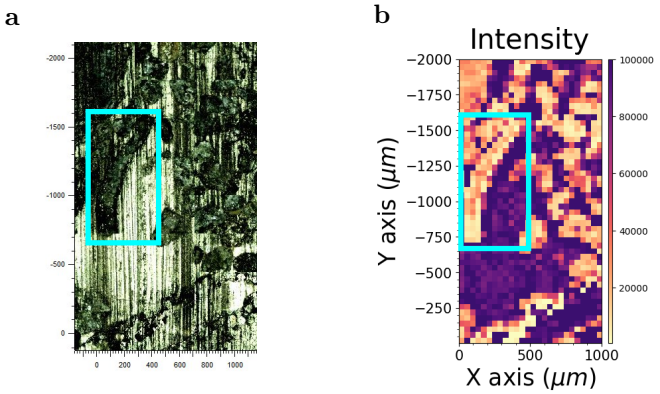

Figure 19: Results of the measurement for the light-blue area of Figure 18a-c. The map and the picture are rotated 180° with respect to Figure 18a-c: **a** Picture of the sample corresponding to the area under study. The area framed in colour is likely to have of char. **b** Map of integrated intensity.

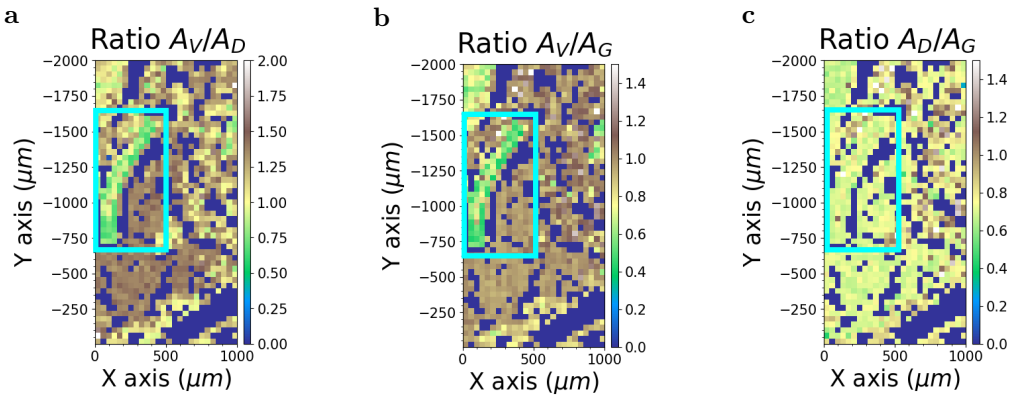

Figure 20: Results of the ratios for the measurement of the light-blue area of Figure 18a-c. The maps are rotated 180° with respect to Figure 18a-c: **a** Map of the A_V/A_D ratio. The zone framed in light blue presents charred organic material. **b** Map of the A_V/A_G ratio. **c** Map of the A_D/A_G ratio.

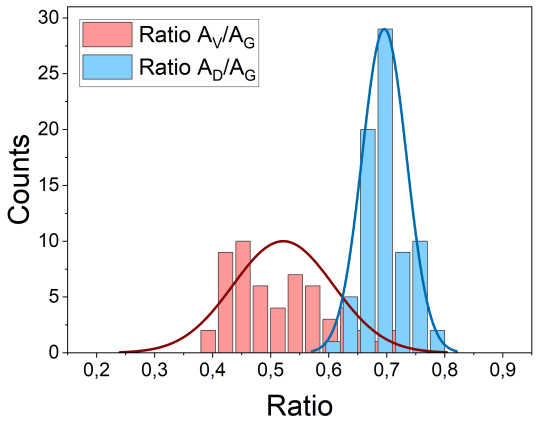

Figure 21: Distribution spectrum for the A_V/A_G ratio values of the light-blue framed area in Figure 20b.

4.1.3 Pink area

The main zones of interest within this area can be seen, framed in pink, in Figure 22a. Figure 22c-d shows the maps of the intensity and the A_V/A_D ratio resulting from the measurements. The intensity map indicates that the main zones of interest lack charred organic material and correspond to saturated or high-intensity points. However, a small area, framed in light blue, presents low intensity values and is, therefore, more likely to have char.

The A_V/A_D ratio for the mentioned area is shown in Figure 22d, where it can aslo be seen framed in light blue. To distinguish the presence of charred material, the spectrum shape for some of the points within the area with ratio values below 1 was studied. Although some of the points do have a char-like spectrum, they are scattered and lack a definite pattern, making it impossible to assure the presence of charred organic matter in the black material of the sample shown in Figure 22b. Further study, involving higher resolution measurements of the area, would be necessary for a more definitive conclusion. This was not done as the area in question falls outside the primary zones of interest. Moreover, this study is primarily focused on developing a more efficient method for identifying char in large samples, rather than targeting exceptionally specific areas with it.

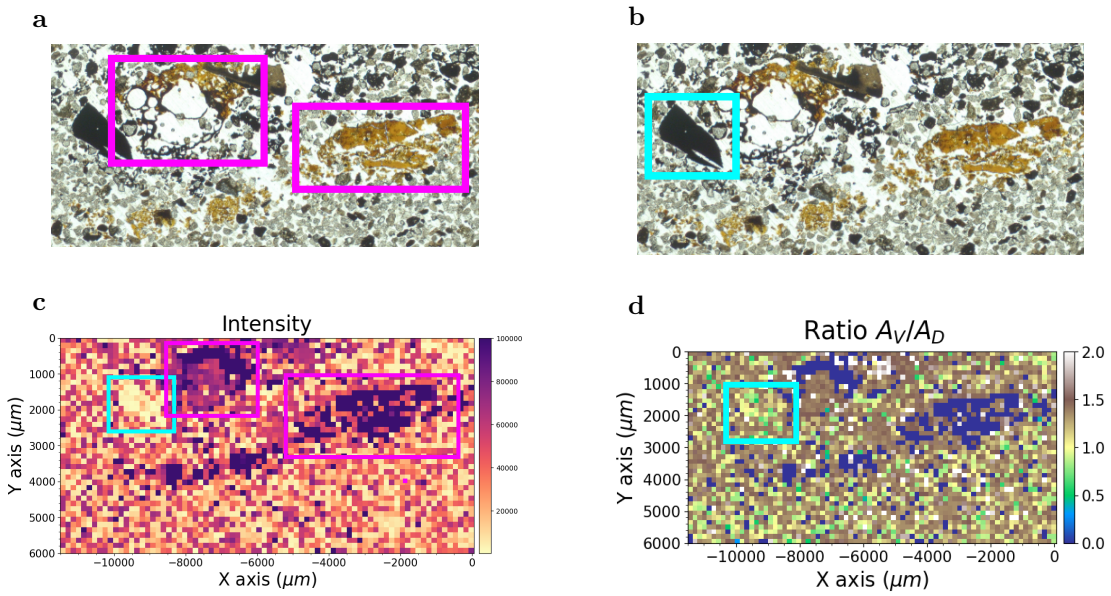

Figure 22: **a** Main zones of interest of the pink-framed area in Sample 1. **b** Zone likely to have char for the same area. **c** Map of integrated intensity. The two main zones of interest are framed in pink. The zone likely to have char is framed in light blue. **d** Map of the A_V/A_D ratio. The area likely to have char is framed in light blue.

4.2 Sample 2

As was done in the preceding section, a summary of the results obtained for the zones in this sample in which the presence of charred organic matter was detected is presented in Table 3. Likewise, throughout this section a comprehensive analysis of the results obtained for each zone wil be made.

Table 3: Values of the A_D/A_G and A_V/A_G ratios for the zones in Sample 2 where charred organic material was found. The last two columns correspond to the peak values of the distribution spectra made with the ratio values for each zone.

Section	A_D/A_G	A_V/A_G	A_D/A_G dist. peak	A_V/A_G dist. peak
Dark blue area	$0.5-0.9$	$0.4-0.8$	0.74	0.57
Green area (High res. measure)	$0.70-0.96$	$0.45-0.91$	0.90	0.73
Red area (High res. measure)	$0.6-0.8$	$0.4-0.7$	0.7	0.55

4.2.1 Light blue area

Results similar to those observed in the pink-framed area of Sample 1 (refer to section 4.1.3) were obtained for this zone. In Figure 23a-c it is shown the intensity and A_V/A_D ratio maps, along with a picture of the zone under study. The absence of a definite area containing charred organic material is evident; instead, numerous scattered points with values of the ratio below 1 and low intensity are observed. Thus, to confirm the presence of char, a more rigorous analysis with higher resolution measures is necessary. As mentioned in section 4.1.3, the main objective of this study is not to identify minute areas of char, so the mentioned analysis was not pursued.

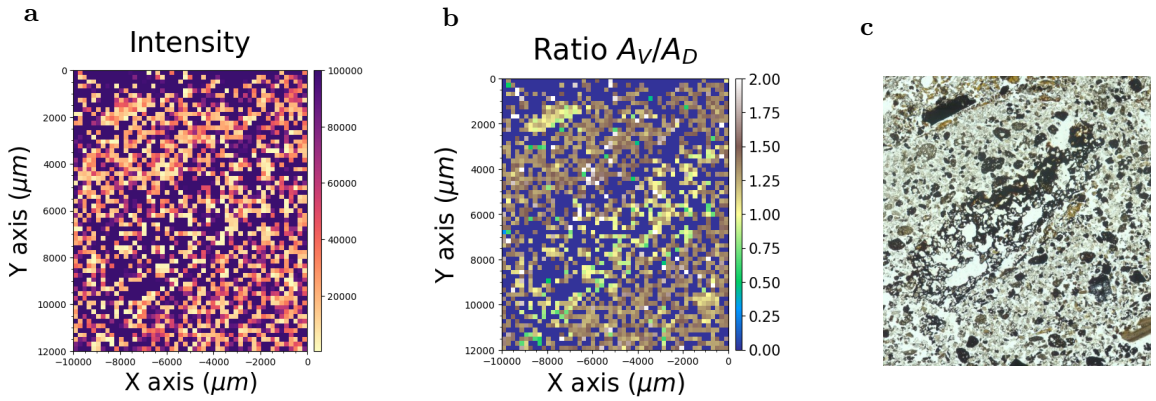

Figure 23: Results for the light blue-framed area in Sample 2. The maps and the picture are rotated 180°with respect to the photograph of the sample (Figure 8): **a** Map of the integrated intensity. **b** Map of the A_V/A_D ratio. **c** Photograph of the respective area.

4.2.2 Dark blue area

Figure 24a-b shows the results which were obtained for this zone. It can be noticed that a small area in the bottom part has low intensity and values of the A_V/A_D ratio below 1 and, hence, has charred organic material. In Figure 24c it can be seen, framed in light blue, the corresponding area in a photograph of the sample.

In Figure 25a-b it can be seen the resulting maps of the A_V/A_G and A_D/A_G ratios, where the same discussed area presents char, although the results for the A_D/A_G ratio are more ambiguous. In Figure 25c, the distribution spectra of both ratios for the area framed in light blue is represented. The A_V/A_G ratio had values between 0.4 and 0.8 with the peak around 0.57, whereas the A_D/A_G ratio had values between $0.5-0.9$, having its maximun at about 0.74.

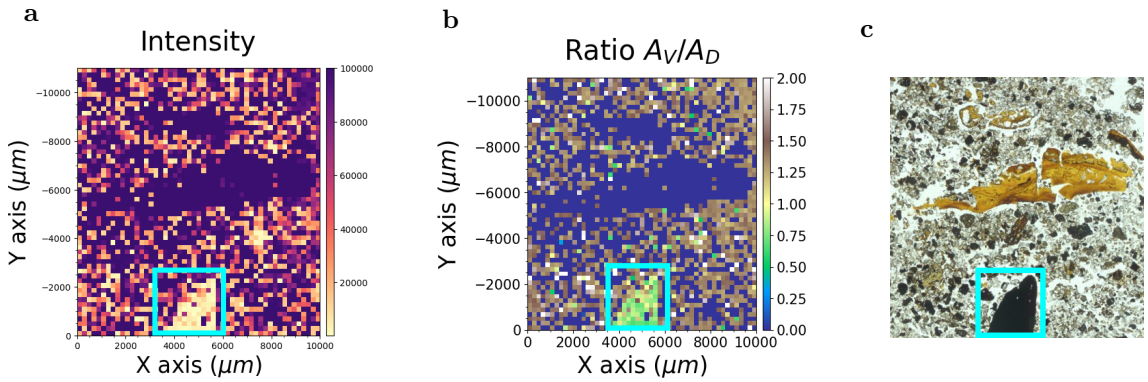

Figure 24: Results for the dark blue-framed area in Sample 2. The light blue-framed zone presents char: **a** Map of the integrated intensity. **b** Map of the A_V/A_D ratio. **c** Photograph of the respective area in the sample.

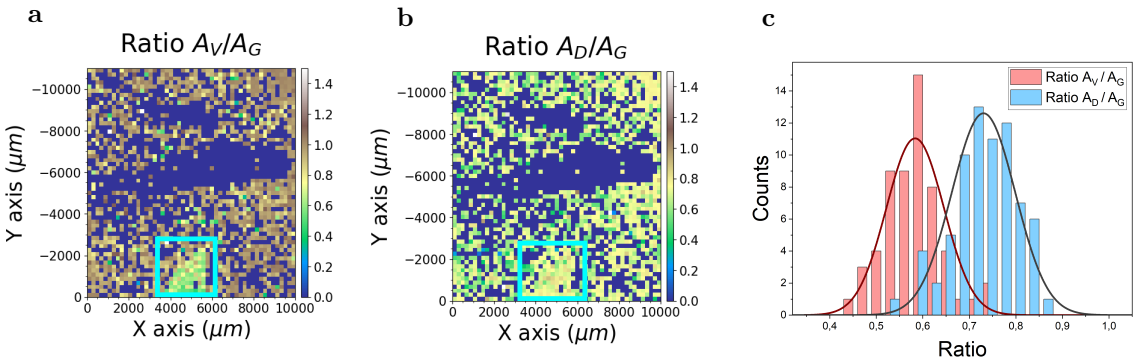

Figure 25: **a** Ratio A_V/A_G of the dark blue-framed area of Sample 2. The zone framed in light blue presents char: **b** Ratio A_D/A_G. **c** Distribution spectra for the mentioned ratios. Each one is represented in a different colour.

4.2.3 Green area

The intensity and A_V/A_D ratio maps for this zone (Figure 26a-b) indicate the possible presence of charred organic material in the upper section. To verify this, a more precise measurement was taken in a specific area within this zone.

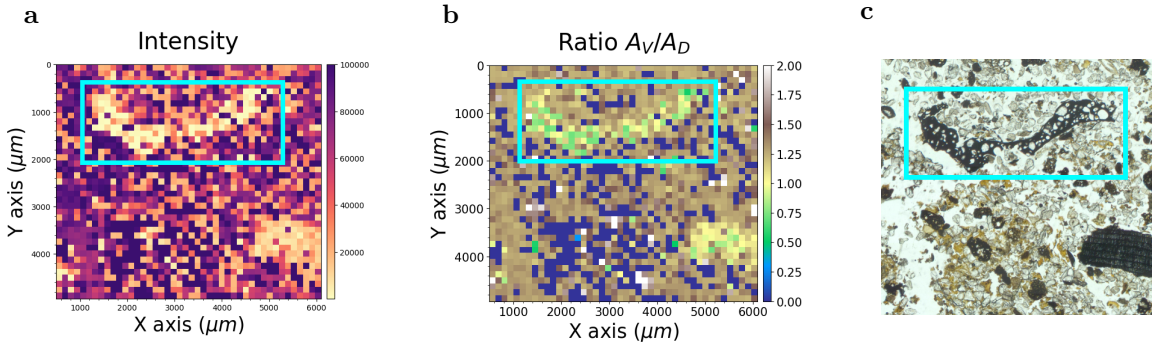

Figure 26: Results for the green-framed area in Sample 2. The light blue-framed zone is likely to have char: **a** Map of the integrated intensity. **b** Map of the A_V/A_D ratio. **c** Photograph of the respective area in the sample.

Figure 27a-b exhibit the results of the intensity map for the aforementioned high resolution measurement, along with a close-up picture of the sample. In Figure 28 the corresponding maps of the ratios are shown. The results of the intensity and the A_V/A_D ratio, as well as those of the A_V/A_G ratio, clearly assure the presence of char in the zone of study. Specifically, the A_V/A_G ratio values ranged from 0.45 to 0.91, being its distribution peak at 0.73 (Figure 29), while the A_D/A_G ratio values ranged from 0.7 to 0.96, with the distribution peak at 0.9 (Figure 29).

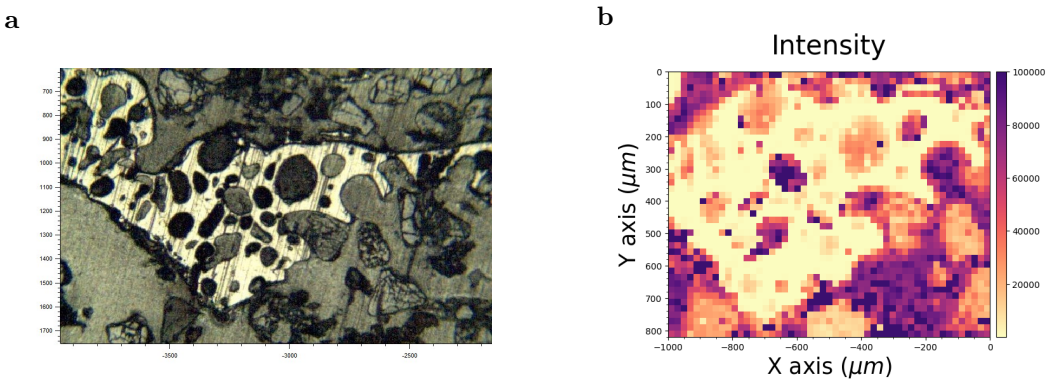

Figure 27: Results of the measurement for the light-blue area of Figure 26a-c: **a** Picture of the sample corresponding to the area under study. **b** Map of integrated intensity.

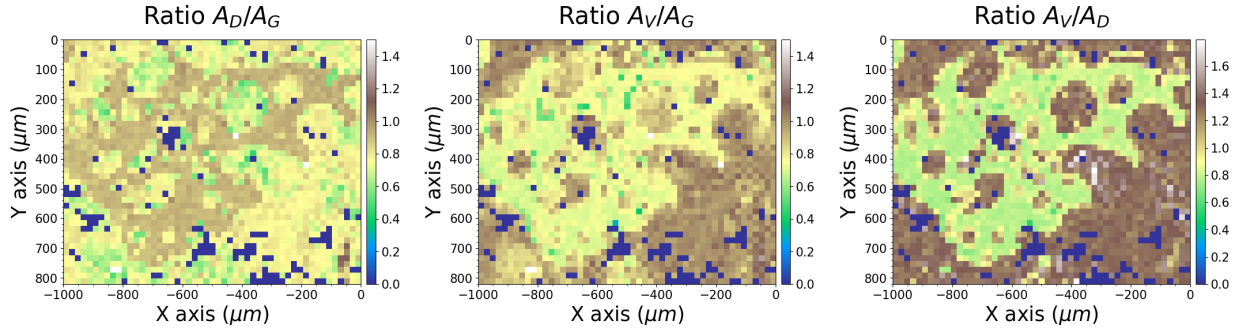

Figure 28: Maps of the A_D/A_G, A_V/A_G and A_V/A_D ratios for the measurement of the light-blue area of Figure 26a-c.

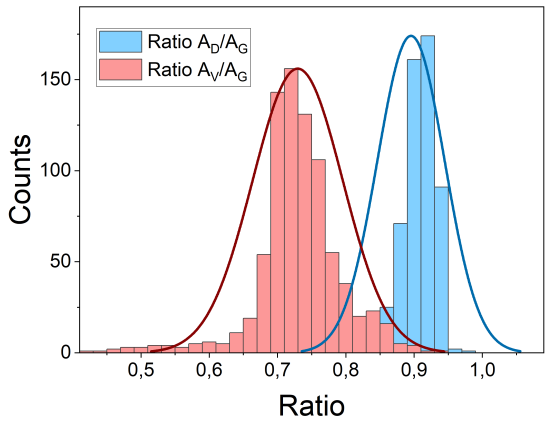

Figure 29: Distribution spectra for the A_V/A_G and A_D/A_G ratios of the high-resolution measurement taken in the light-blue framed area of Figure 22a-c.

4.2.4 Red area

The main results for this zone are exhibited in Figure 30. As in the previous case, it can be appreciated an area on the upper section which might present charred organic matter. The results of the higher-resolution measurement taken on this area are shown in Figure 31a-e. Finally, the distribution spectra of the A_V/A_G and A_D/A_G ratios is represented in Figure 32. The values obtained for A_V/A_G ratio ranged between approximately 0.4 and 0.7, being the maximum value at about 0.55. In the other hand, the A_D/A_G ratio had values between 0.6 and 0.8, approximately, with the maximum value being 0.7.

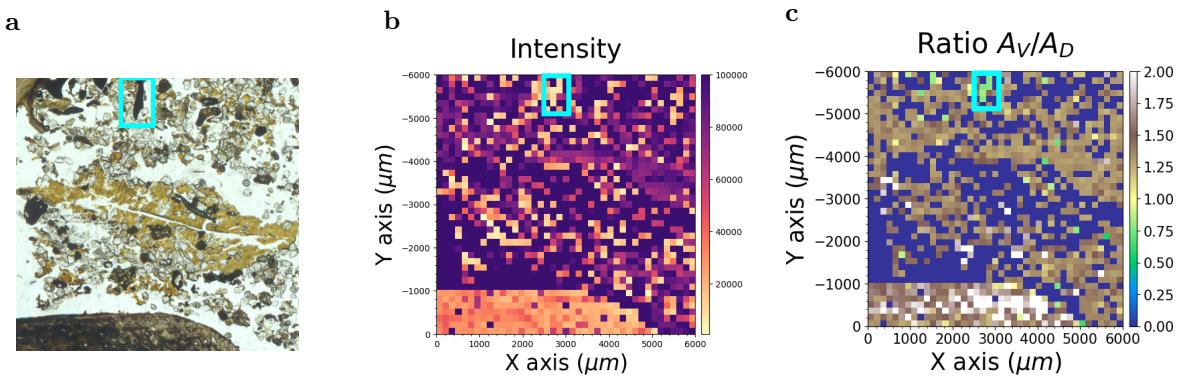

Figure 30: Results of the measurement of the red-framed zone in Sample 2. The area which can be seen framed in light-blue is likely to have char: **a** Picture of the zone. **b** Intensity map. **c** A_V/A_D ratio map.

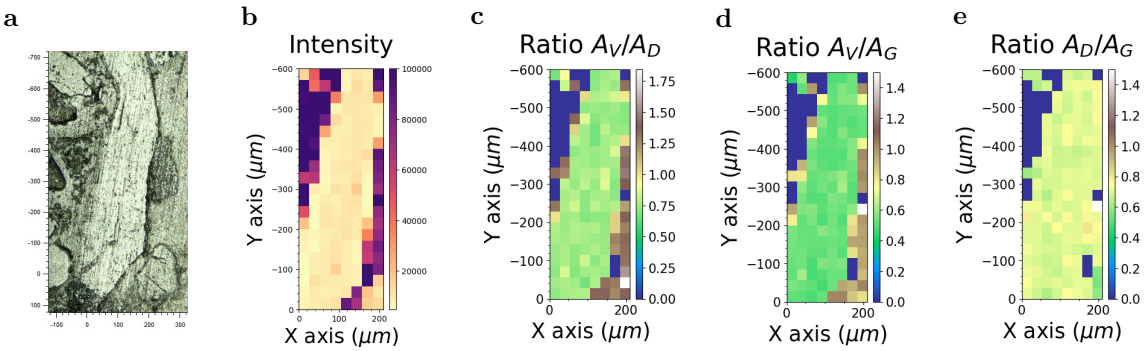

Figure 31: Maps resulting of the measurement taken in the light blue-framed area of Figure 30a-c: **a** Picture of the area. **b** Intensity map. **c** A_V/A_D ratio map. **d** A_V/A_G ratio map. **e** A_D/A_G ratio map.

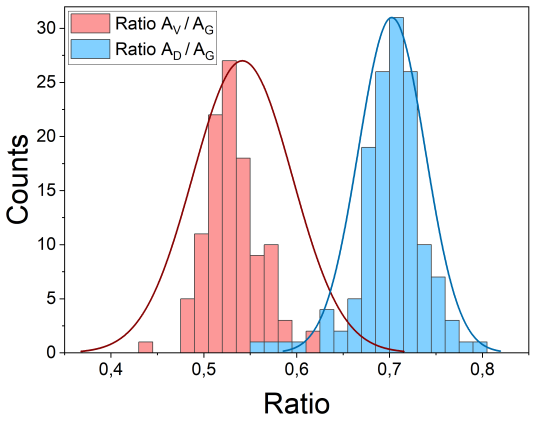

Figure 32: Distribution spectra for the A_V/A_G and A_D/A_G ratio results shown in Figure 31d-e of the ligh blue-framed area in Figure 30a-c.

5 Discussion

Resumen

En esta sección, se lleva a cabo un análisis de los resultados presentados anteriormente con el objetivo de clasificar la naturaleza de la materia orgánica carbonizada encontrada, determinando si corresponde a origen animal o vegetal. Para lograr esto, se realiza una comparación entre los valores de los ratios obtenidos y los rangos establecidos por Lambrecht et al. (2021) [12] como diferenciación entre origen animal y vegetal.Este proceso se aplica a cada muestra individualmente. Además, se lleva a cabo una discusión general de los resultados, donde se analizan posibles factores metodológicos y características propias de las muestras que podrían haber influido en los resultados obtenidos.

In the following sections, the differentiation between plant and animal-derived matter in our samples will be discussed, considering the results obtained by Lambrecht *et al.* (2021) [12], which were covered in section 1.

5.1 Sample 1

Table 2 provides a summary of the results obtained from this sample. Subsequently, a detailed analysis will be conducted for each area of interest in Sample 1 to differentiate whether the nature of the organic matter found corresponds to animal or plant origin.

Starting with the red-framed zone within the yellow-framed area (Figures 15a-b and 16a-b), when examining its outcomes it was found that the peak value of the A_D/A_G distribution spectrum is 0.67 (Figure 16b). While this value is almost below the lower limit of animal-derived matter, it is not possible to determine if the source is animal or plant-based, given the ranges identified by Lambrecht *et al.* (2021) [12] and exhibited in Table 1. In contrast, the distribution spectrum of A_V/A_G revealed a peak value of 0.46 (Figure 16a), which falls unequivocally within the range indicative of plant-derived matter. Futhermore, upon considering the complete range of the distribution spectra instead of just the peaks, it is noticeable that the A_D/A_G values demonstrate a tend towards low values of the ratio, thus falling within the range which corresponds to plant-derived organic matter. A similar pattern is observed when considering the entire range of the A_V/A_G ratio. Consequently, it can be safely concluded that the charred organic matter discovered in this zone is of plant origin.

Focusing on the results of the blue-framed zone within the same area, the A_D/A_G distribution spectrum had its peak at 0.81 (Figure 16b). Unlike the previous case, this value is almost above the upper limit of the range indicative of plant-derived matter, but falls well within the range corresponding to animal-derived matter. Therefore, it is again not possible to differentiate between animal or plant-derived origin based solely on this result. Otherwise, the peak of the A_V/A_G distribution spectra was found at 0.63 (Figure 16a), which is clearly within the range for animal-derived matter, in spite of being also close to the upper limit of the range for plant-derived matter. In this case, the complete ranges of both distribution spectra values do not help to clarify the differentiation. However, considering the maximun concentration of Lambrecht *et al.* (2021) [12] results for plant-derived matter, which is located within the range $0.5-0.65$ (as mentioned in section 1), it becomes less likely that the peak of the A_D/A_G distribution spectrum (0.81) corresponds to plant-derived matter. This, along with the result for the A_V/A_G ratio, makes it possible to conclude that the charred organic material detected in the blue-framed zone has animal origin.

Regarding the outcomes obtained from the orange-framed zone of the yellow-framed area, the A_D/A_G distribution spectrum exhibited a peak value of 0.63 (Figure 17), which is consistent with plant-derived matter. Analysis of the complete distribution spectrum shows that although some higher values of the A_D/A_G ratio may fall within the range of animal-derived matter, the highest concentration is centered around and mainly below 0.65, indicating a plant-based origin. Moreover, a distribution peak of 0.3 was found for the A_V/A_G ratio (Figure 17), being this value also within the range of plant-derived matter and thus confirming that the charred organic material of this zone is of plant origin. However, it is worth noting that the entire dataset of the A_V/A_G ratio for this zone extends to very low values, as low as 0.2, which is outside the inferior limit found by Lambrecht *et al.* (2021) [12]. Therefore, it may be worthwhile to conduct further extensive and specific research in this area of the sample to fully understand the implications of these low ratios.

Finally, with respect to the black-framed area of Sample 1 (Figure 7), the results obtained for the high resolution measurement revealed a peak value of 0.7 in the A_D/A_G distribution spectrum (Figure 21). This value falls within the indicative range of both animal and plant-derived matter. Moreover, upon analyzing the entire distribution range, it is evident that the data does not exhibit a tendency towards either extreme, and as a result, it cannot be conclusively identified as either animal or plant-derived. Similarly, the A_V/A_G ratio exhibited a peak value of 0.55, which falls within the range

indicative of animal-derived matter but, while it is close to the upper limit of the range for plant-derived matter, it is still whithin it, and hence it is not possible to definitively determine its nature. Examining the complete set of distribution data, it can be appreciated that, although the distribution curve starts at a value around 0.25, the data begins at almost 0.4 and trends towards higher values, up to 0.8. This tendency suggests an animal-based origin for the charred organic material detected in this zone. However, this evidence is not conclusive enough to classify it unequivocally, and thus this area remains undefined.

5.2 Sample 2

The outcomes obtained for the zones of interest in this sample where char was detected are recapped in Table 3. Next, following the analytical methodology applied in the preceding section, a thorough analysis for every zone listed in the table is presented with the aim of differentiating their nature.

To begin with, the dark blue area (shown in Figure 8) presented ambiguous values for the peaks of the distribution spectra of the A_D/A_G and A_V/A_G ratios. With regard to the A_D/A_G ratio, the peak of the distribution exhibited a value of 0.74 (Figure 25c), which is within the range indicative of both plant-derived and animal-derived matter. Hence, it is not possible to discern the origin with certainty. Additionally, considering the complete range of the distribution values for this ratio and not just the peak, it is noticeable that there is not a predominancy between high or low values, the data falls in the middle of both ranges exposed by Lambrecht *et al.* (2021) [12] and summarized in Table 1. Thereby, this ambiguity also precludes the distinction of the nature of the material found in this area. Similarly, the A_V/A_G ratio values exhibit the same aforementioned limitation. The peak was found at a value of 0.57, which is proximal to the upper limit of the range indicative of plant-derived matter but also falls well within the range corresponding to animal-derived matter. However, its presence within both ranges makes it impossible to classify its origin. Furthermore, the entire set of distribution values encompasses again a significant portion of both ranges specified by Lambrecht *et al.* (2021) [12]. As a result, this distribution does not aid in clarifying the nature of the material present in the area either. Therefore, although initially this measurement appeared to offer clear and conclusive values for the ratios, it may be necessary to take a higher-resolution measure in the small zone with presence of charred organic material to better distinguish its nature, similar to what was done in other areas where it was found.

Regarding the light-blue zone of the green-framed area (Figure 26a-c), the distribution spectrum of the A_D/A_G ratio presented a peak value of 0.9 (Figure 29), which falls within the range corresponding to animal-derived matter. Although this value is close to the limit of plant-derived matter, further analysis of the complete distribution spectrum reveals that the majority of the values are concentrated between 0.85 and 0.95, with only a few values as low as 0.7. Therefore, it can be unequivocally determined that the ratio values represent animal-derived matter. Furthermore, the distribution peak of the A_V/A_G ratio was determined to be at 0.73, which also falls within the range corresponding to animal-derived matter. This finding is, again, further supported by the complete spectrum analysis. Thus, it can be concluded that the organic matter found in this area is of animal origin.

Focusing on the outcomes of the higher-resolution measurement taken in the red-framed area in this sample (Figure 31a-e), a similar situation to that of the dark blue area is observed. Specifically, a distribution peak value of 0.7 was found for the A_D/A_G ratio (Figure 32), falling within the ranges corresponding to both plant and animal-derived matter. In addition, the distribution spectrum is narrow and well centered around 0.7, which does not allow to clarify the conclussion when basing on the complete set instead of the peak. Moreover, it was obtained a peak value of the A_V/A_G distribution spectrum of 0.55, which is also indicative of both origins (plant and animal). A similar pattern to that observed in the A_D/A_G ratio is noticeable in relation to the width of the distribution spectrum. Although it is slightly less narrow, it is still well-centered around the peak, with no predominance of one side with higher counts of the ratio values. Consequently, this ratio does not help to discern the nature of the organic charred material either and thus remaining undefined.

5.3 General discussion

With the aim of enhancing the clarity of the results just discussed, a summary of the same is provided in Table 4 and Figure 33a-b. The areas of Sample 1 yielded more conclusive outcomes when studying their nature, while those of Sample 2 were challenging to characterize, with the majority remaining indistinct in their origin.

Specifically, the A_V/A_D ratio was the most effective to identify the presence of charred organic material. Otherwise, the A_D/A_G ratio frequently produced uncertain results that limited the classification of the material. Typically, the distinction between the two origins (plant or animal) was made by analyzing the A_V/A_G values. However, while

some results could be assigned to one nature or the other, the majority exhibited values that were a bit ambiguous or approached the threshold of the other origin.

Table 4: Results of the differentiation for the nature of the zones, in both Sample 1 and Sample2, where charred organic material was detected. The term "High res. measure" refers to the results of a high-resolution measurement taken in a small zone of the corresponding area where the presence of charred organic material was likely, to confirm its existence.

Sample	Zone	Origin
Sample 1	Red framed zone (Yellow area)	Plant
	Blue framed zone (Yellow area)	Animal
	Orange framed zone (Yellow area)	Plant
	Black area (High res. measure)	Undefined
Sample 2	Dark blue area (High res. measure)	Undefined
	Green area (High res. measure)	Animal
	Red area (High res. measure)	Undefined

One possible explanation for this ambiguity in the results is the presence of noise in the Raman spectra. In their study, Lambrecht *et al.* (2021) [12] investigated highly smoothed spectra by acquiring two sets of 57 and 108 spectra, respectively, at points where the presence of char was confirmed. This approach facilitated precise determination of the positions of the D and G band peaks and of the valley, thus allowing for accurate calculation of the different ratios. Nonetheless, in the present study, since large areas were investigated rather than specific points, the spectra obtained were significantly noisier due to the acquisition of sets of only 2 spectra per point, as previously noted in Section 3.3. To minimize the noise in the signals, a smoothing filter was applied, and the ratios were calculated by integrating over areas rather than using single point values.

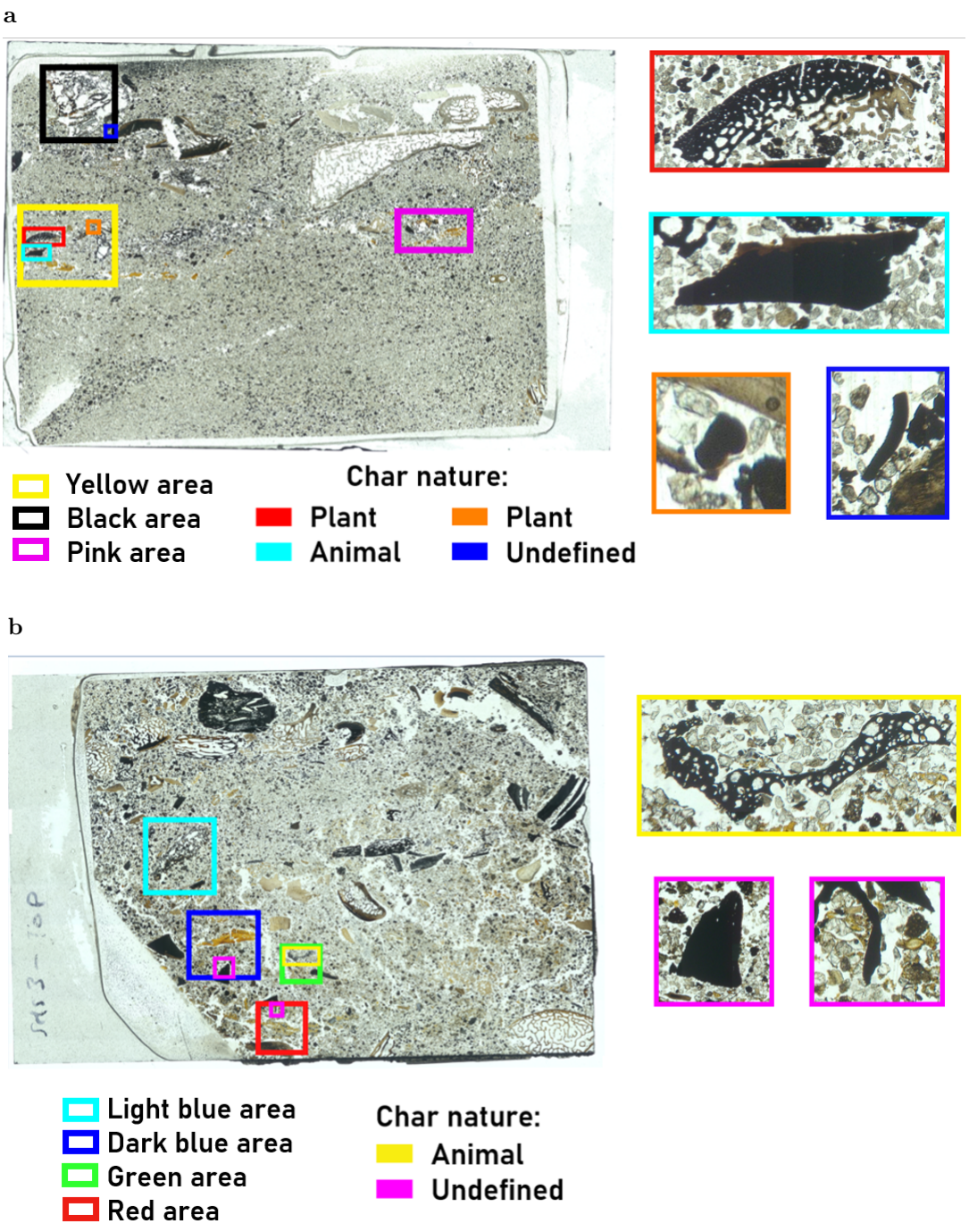

Figure 33: Results of the differentiation for the nature of the zones in the areas of interest within the samples where char was detected: **a** Results obtained for Sample 1. **b** Results for Sample 2.

However, this procedure may not be sufficient to counteract the effects of noise, as many spectra may not exhibit well-defined D and G band peaks and valley, or may display peaks within the valley due to noise, or may exhibit altered spectral shapes due to various factors such as the effect shown in Figure 10b. Consequently, the calculated areas may result in unclear results for the ratios. Thereby, in future studies, when taking the higher-resolution measurements to clasify the charred organic material found, it would

be advisable to increase both the integration time and the number of spectra acquired per point. In so doing, the signal noise will be lesser and may help counteract some of the aforementioned effects, yielding more accurate results.

Another potential reason for the ambiguity in the results could be the misalignment of the samples when taking the measurements. As described in section 3.1, the sample support consists of a single 3D-printed piece with two thin protrusions on either side, on which the sample rests, and three screws which enable adjustment of the sample and which mantain its stability. However, the two mentioned protrusions are not perfectly flat, which makes it difficult to position the sample so that it remains level. Furthermore, the glass of the samples has very thin borders that can present imperfections, making it challenging to adjust the screws, particularly when employing foam to prevent its deterioration. At times, the vertical cuts on the sample borders can make it impossible to adjust the screw and cause the glass to slide above or under it. Additionally, the horizontal notches on the glass do not let to adjust well the screw, resulting in a loose and wobbly sample. All of these small factors contribute to the sample becoming inclined and prevent the achievement of a perfectly flat sample placement. However, imperfections of the samples themselves should also be considered, as the cutting into thin sections is not always perfect, which can result in a surface that is not completely flat. In addition, since the precision of the microscope makes it to be very sensitive to small variations, even slight changes in the sample height can cause it to become out of focus. Hence, due to all the factors previously mentioned, achieving a perfect focus of the samples during the measurements was difficult. As a result, most of the times the samples appeared slightly blurry, as the microscope's Z-position was set to the middle point between the smallest and highest Z-values in the area under study, in an attempt to maintain consistent focus across the entire area. This blurring may have adversely affected the spectral resolution, resulting in more noise in certain areas, as well as the height and definition of the peaks. This could have led to ambiguous results of the areas and, consequently, of the ratios. Thereby, for future studies, it would be convinient to design an improved support which minimizes the effects of improper sample placement, so that we only have the effects of the imperfections on the sample surface, which would enable more precise measurements with better focus.

To conclude, notwithstanding the discussed ambiguity in some of the results, the majority of the main objectives of this study have been succesfully achieved. The experimental method followed was effective in detecting the presence of charred organic material in both of the analyzed samples. Thus, this method offers a new, faster and

more convenient approach to identifiying char, not only when large areas of samples need to be studied, but also in small regions if the appropiate resolution is selected for the measurement. Moreover, while it is true that the initial results obtained for the areas were inconclusive, needing to take smaller measurements on the zones likely to present char, this issue could be addressed by adopting different approaches: increasing the integration time for the measurements, taking a larger number of spectra at each point, performing higher-resolution measurements from the outset, or implementing a combination of these techniques. Overall, the results obtained align with the study's intended objectives and could be considered satisfactory.

6 Conclusions

Resumen

En esta sección final, se destacan los principales logros y limitaciones del trabajo realizado, además de proporcionar posibles enfoques para futuras investigaciones que puedan mejorar los resultados obtenidos y el método propuesto, aumentando su eficiencia y precisión.

It has been demonstrated that the proposed experimental methodology is efficient in identifying char in large samples. This can be done more effectively by attending to the intensity values along with the A_V/A_D ratio. Hence, the presented method may facilitate and expedite the interpretation of archaeological samples, allowing for better selection of those to focus on. Aditionally, in the majority of the cases, it has enabled the differentiation of the nature of the charred organic material.

Nonetheless, further investigation in this area is required. The only approach to differentiating charred organic material nature by the use of the ratios between the Graphite and the Disorder areas is the one developed by Lambrecht *et al.* (2021) [12]. Hence, with more specific and comprehensive research in this field, accumulating more data, defining clearer boundaries between the two origins, and possibly establishing a correlation between D/G and V/G ratios, it is possible that the method here developed will accomplish both the identification of char and the distinguishion of its nature. Future studies could also explore the use of V/D ratio calculations, which, as seen in this study, provide an excellent idea of where char is present. In addition, with further investigation on the effects which can influence on the values of these ratios, such as the temperatue or the resin used on the samples preparation, the results can be better comprehended and, thus, a more precise differentiation could be made.

References

[1] Robin R Jones et al. "Raman techniques: fundamentals and frontiers". In: *Nanoscale research letters* 14.1 (2019), pp. 1–34.

[2] Ruchita S Das and YK Agrawal. "Raman spectroscopy: Recent advancements, techniques and applications". In: *Vibrational spectroscopy* 57.2 (2011), pp. 163–176.

[3] T. Editors of Encyclopaedia Britannica. "Raman effect". In: *Encyclopedia Britannica* (2022).

[4] Kang Soo Lee et al. "Raman microspectroscopy for microbiology". In: *Nature Reviews Methods Primers* 1.1 (2021), p. 80.

[5] James Jonkman et al. "Tutorial: guidance for quantitative confocal microscopy". In: *Nature protocols* 15.5 (2020), pp. 1585–1611.

[6] Gregory D Smith and Robin JH Clark. "Raman microscopy in archaeological science". In: *Journal of archaeological science* 31.8 (2004), pp. 1137–1160.

[7] Howell GM Edwards and Peter Vandenabeele. *Raman spectroscopy in art and archaeology*. 2016.

[8] Concepción Domingo. *Técnicas de espectroscopía Raman aplicadas en conservación*. 2011.

[9] Danilo Bersani et al. "Methodological evolutions of Raman spectroscopy in art and archaeology". In: *Analytical Methods* 8.48 (2016), pp. 8395–8409.

[10] Howell GM Edwards, Peter Vandenabeele, and Philippe Colomban. In: *Raman spectroscopy in cultural heritage preservation*. Springer Nature, 2022. Chap. Chapter 1: Introduction, pp. 1–2.

[11] D. Deldicque et al. "Effects of oxidative weathering on Raman spectra of charcoal and bone chars: consequences in archaeology and paleothermometry". In: *Comptes Rendus. Géoscience.* 355(G1) (2023), pp. 1–22.

[12] G. Lambrecht et al. "Characterisation of charred organic matter in micromorphological thin sections by means of Raman spectroscopy". In: *Archaeological and Anthropological Sciences* 13 (2021), pp. 1–15.

[13] Jean-Noël Rouzaud et al. "Carbons at the heart of questions on energy and environment: A nanostructural approach". In: *Comptes Rendus Geoscience* 347.3 (2015), pp. 124–133.

[14] L. Leierer, C. Rodríguez, and C Mallol. "Micromorphological thin section manufacture AMBI Lab, Universidad de La Laguna, Tenerife, Spain". In: *protocols. io* (2019).